Soumis le : 25/06/2016
Forme révisée acceptée le : 22/01/2017
Auteur correspondant : hbendjebbas@gmail.com

Nature & Technology

Mathematical model of heliostat reflective surface deformation

BENDJEBBAS Hichem[a], ABBAS Mohamed[a], EL-HADJ ABDELLAH Abdellah [b], SELLAMI Rabah[a], MGHAZZI-LAARAFI Mohamed[a]

[a] *Unité de Développement des Equipements Solaires. UDES. Centre de Développement des Energies Renouvelables. CDER, Bou-Ismail. 42415.W. Tipaza, Algerie*

[b] *Laboratoire de Mécanique, Physique et Modélisation Mathématique. LMP2M, Université de Médéa, 26000 Médéa, Algérie*

Abstract

Optimum design of isolated units or fields of heliostats is depend upon obtaining realistic design of wind loads, gravity loads and thermal stresses. The stationary and dynamic effects of wind will be an important factor for heliostats. Some experts have conducted a series of field measurements and wind tunnel tests for determining different wind load configurations on heliostats. A monitoring program covered six-year period from 1986 to 1992 which focused on the issues of heliostat beam quality, mirror module performance and durability, tracking accuracy, dynamic wind effects, and overall operational and maintenance characteristics. The present work is a simplified method of estimating the deformation of heliostat due to gravity loads and thermal stresses and static wind loads by establishing a mathematical model of different loads affecting the deformation of heliostat reflective surface modules.

Keywords: CSP, Heliostat, wind loads, gravity loads, thermal stresses.

1. Introduction

By making an inventory of the development of heliostats and their market listing in the future with their specific weight and cost, respectively, the development will be from rigid and heavy construction towards lightweight construction and low cost. Currently, two configurations seem beings heliostats cheap solutions (Fig.1), (a) rectangular heliostat (e.g. GM-100) and (b) circular stretched membrane heliostat (e.g. ASM-150). Similar prototypes configurations of heliostats were tested, but it is too early to say what the best solution [1].

Reducing the specific cost of the heliostat by simplifying the supporting structure, reducing its weight and move towards the larger sizes of heliostats has a contradictory effect on the quality of the reflected sun rays image [3].

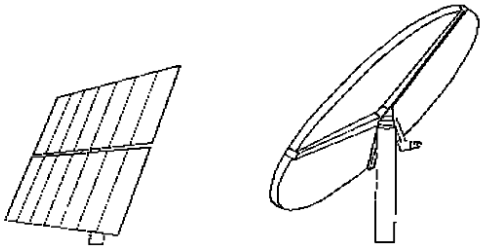

a: GM-100 b: ASM-150

Fig.1: Heliostats [2]

Fig.2: Heliostats solar power tower field [2]

Increasing the pointing error or the error of the reflected image of an entire heliostat field (Fig.2) also augment the production cost of the plant turn. In order to check the optical performance of the heliostat, it is necessary to know the sources of error and then quantify them.

2. Error source:

On a reflecting surface, the reflectance of the normal angle of any point is equal to the angle of incidence. However, in the applications of concentrating solar systems, the direction of the normal of the solar concentrator (heliostat) surface is not always exactly known. The normal of the surface of a heliostat facet at a given point deviates from its ideal position because of several parameters: undulations of the surface of the facets, errors of orientations due from oscillations and by structural deformation due from gravitational loads, wind loads and influence of temperature. The reflected rays are shifted from central ray (pointing error) or, in the case where the entire hub is misaligned; the central beam is reflected at various points (tracking error) [4]. The total dispersion error of the reflected beam distribution can be written as:

$$\sigma_{total}^2 = \sigma_{sun}^2 + \sigma_{aber.}^2 + \sigma_{BQ}^2 \qquad (1)$$

where: σ_{sum} is the sun shape error, σ_{aber} is the optical aberration error of heliostat facets and σ_{BQ} is the beam quality error of the reflected sun rays. The required value of σ_{BQ} is 2 to 2.6 *mrad*.

The optical errors contribution in the dispersion of the reflected beam can be written as follows:

$$\sigma_{BQ}^2 = \sigma_{ondul.}^2 + \sigma_{ocsil.}^2 + \sigma_{cg}^2 + \sigma_{temp.}^2 + .. \qquad (2)$$

The deterioration of the reflected beam quality due to gravity loads and temperature effect will be the subject of this study by the determination of the mathematical model deformation of the heliostat reflecting surface.

3. Heliostat geometry:

In order to estimate the deformations of heliostat reflective surface, we will study a significant size heliostat.

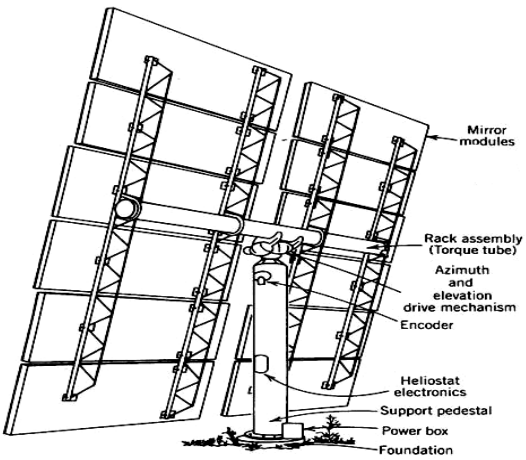

Fig.3: A 105 m^2 heliostat

The Net reflection surface of the heliostat (Fig.3) is 105 m^2 composed by 32 facets of 1.1x3 *m* supported by 08 trusses of 9 *m* length, all mounted on a torque tube of 12.4 *m* in length and with a diameter of 0.4 *m*, this assembly is mounted on the azimuth and elevation drive mechanism in

the central portion of the torque tube. All these components are rigidly fixed on a support pedestal with 04 *m* in length and a diameter of 0.61 *m*.

4. Mathematical model:

To describe mathematically the behavior of the heliostat reflective surface deformation, some basic definitions are useful. The coordinates system used in this model has its origin in the center (reflective surface). (Fig.4)

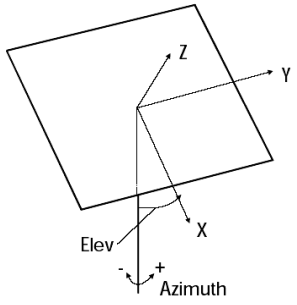

Fig.4: Coordinates system of heliostat

The elevation angle is called (elev.) and equal to zero when the facets are in the vertical position. The azimuth angle is zero when the heliostat is directed to the south, positive in east and negative in west. The calculation of heliostat reflective surface deformation with very complex geometries requires very powerful simulation tools, however, it is possible to simplify the calculations by isolating the components of the heliostat one by one (by applying the different loads such as: gravity loads, temperature, ...). This method allows us to estimate the deformation due to different loads (gravity, temperature...) and in the end linearly superposed [5].

4.1. Gravity loads:

4.1.1. Gravity loads on the support pedestal:

The simplified geometry of the pedestal can be seen in (Fig. 5). It consists of a 4 000 *mm* long (L_{ped}) steel tube with an outer diameter D_{ped} of 600 *mm* and a thickness t_{ped} of 16 *mm*. it is rigidly mounted on a concrete foundation. On a top of the pedestal is the elevation drive that moves the torque tube with the help of a lever of the length *e*. The weight of facets, trusses and torque tube induce the force $F_{conc.}$

$$F_{conc} = (m_{facets} + m_{trusses} + m_{tube}).g \quad (3)$$

This force causes the moment:

$$M_{b,ped} = F_{conc}.e.\cos(elev + 60°) \quad (4)$$

The additional angle of 60° comes from the mounting geometry (Fig.5). The moment $M_{b,ped}$ changes with the elevation angle and has the same value over the whole length of the pedestal. This causes the tube to tilt forward about the angle.

$$\Delta elev = \frac{M_{b,ped}.L_{ped}}{E.I} \quad (5)$$

with E: Young's modulus and I the Moment of inertia. The resulting *Z-displacement* of the mirror plane is:

$$\Delta z_{ped,g}(x) = -\Delta elev.x \quad (6)$$

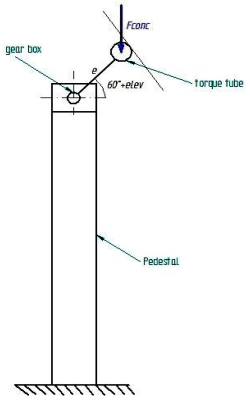

Fig.5: Pedestal geometry

4.1.2. Gravity loads on the torque tube:

4.1.2.1. Bending:

The simplified model of the torque tube is shown in (Fig.6). Its geometry and loads are supposed symmetrical. There is an inner moment $M_{b,tube}$ in the cutting plane that needs to be considered in order to satisfy the equilibrium of forces and moments. The boundary conditions of the tube given mathematically are $z'(0)=0$ and $z(0)=0$ per definition of the coordinate system. The steel tube has a thickness of $t_{tube}=16\ mm$, an outer diameter of $D_{tube}=406\ mm$ and its half length $L_{tube}/2=6200mm$. The support is in the distance of $l_{bending}=500\ mm$ and the trusses are mounted in the distances l_1 to l_4.

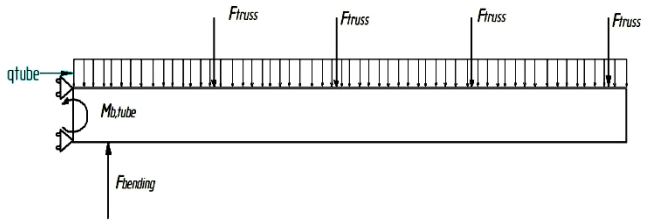

Fig.6: Simplified model of one side of torque tube

The weight of the facets and the trusses induce the forces:

$$F_{truss} = -(m_{4\,facets} + m_{1truss}).g \tag{7}$$

While the weight of the tube itself is modeled as the area load q_{tube}:

$$q_{tube} = -A_{tube}.\rho_{steel}.g \tag{8}$$

From the equilibrium of forces it is known that the reaction force in the bearing is:

$$F_{bearing} = -(4.F_{truss} + q_{tube}.\frac{L_{tube}}{2}) \tag{9}$$

From the equilibrium of moments results the inner moment

$$M_{b,tube} = -F_{truss}.(l_1 + l_2 + l_3 + l_4) - F_{bearing}.l_{bearing} - \frac{(L_{tube}/2)^2.q_{tube}}{2} \tag{10}$$

The equation of the bending line of the torque tube is:

$$w(x) = -\frac{1}{E.I}.\left[\frac{M_{b,tube}}{2}.x^2 - \frac{F_{bearing}}{6}\left\{x - l_{bearing}\right\}^3 - \frac{F_{truss}}{6}\left(\left\{x-l_1\right\}^3 + \left\{x-l_2\right\}^3 + \left\{x-l_3\right\}^3 + \left\{x-l_4\right\}^3\right) - \frac{q_{tube}}{24}x^4\right] \tag{11}$$

The displacements in z-direction of the facets are independent of the distance from the tube (y), but depend on the distance in x-direction and elevation angle:

$$\Delta z_{tube.bending,g}(x) = \sin(elev).w(x) \tag{12}$$

4.1.2.2. Torque:

The center of gravity of the concentrator is not located in the axis of the tube, but at the distance a from the axis. The facets are mounted close to tangential to the torque tube, hence the distance a is supposed to be the radius of the torque tube.

$$M_{truss} = m_{4\,facets}.g.a\cos(elev) \tag{13}$$

By calculating the twisting angle φ of the torque tube in the distance x:

$$\Delta z_{tube,torque,g}(x,y) = \sin(\varphi(x)).y \tag{14}$$

4.1.3. *Gravity loads on the trusses*:

The trusses form plane frames as shown in (Fig.7). The weight of the facets and the trusses themselves are added up to a single area load q_{truss} that acts over the whole length.

$$q_{truss} = \frac{m_{1truss}}{L_{truss}} \tag{15}$$

The structure is fixed to the torque tube that is assumed to be ideally rigid.

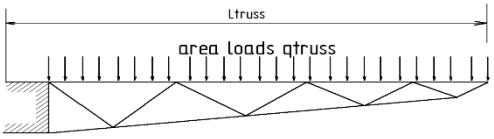

Fig.7: Simplified model of the truss

The forces, stresses and deformations of all the bars can be calculated by the equations of pin-jointed frames [7]. Once the deformations of the bars are known, the deformation of the whole truss can be determined.

$$\Delta z_{truss,g} = (0.0095.|x|^3 - 0.1288.x^2 - 0.0404|x|).\sin(elev) \quad (16)$$

4.2. Temperature influence:

The changing ambient temperature does not affect the shape of the support structure, whereas the spatial temperature gradient due to solar insolation does. All parts facing the sun will heat up while the parts in the shade stay cooler. The resulting temperature differences make the front side expand more than the backside and hence the structure bends out of shape [1], [6]. The only parts of the GM-100 support structure that are exposed to direct sunlight are the pedestal and the torque tube. Therefore it is sufficient to find a model for bending of tubes as shown in (Fig.8).

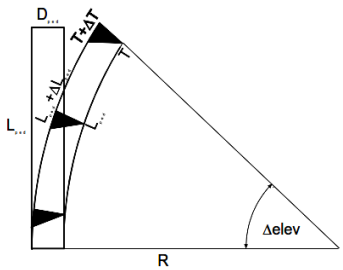

Fig.8: Bending of a tube due to a temperature gradient

The warmer side expands about the length ΔL_{ped} while the cool side keeps its temperature and length .

$$\Delta L_{ped} = L_{ped}.\Delta t.\alpha \quad (17)$$

with α: temperature coefficient of steel. This causes the tube to bend in an arc with radius R and the resulting tilting angle Δ_{elev} in radians is:

$$\Delta_{elev} = \frac{L_{ped}}{R} = \frac{\Delta L_{ped}}{D_{ped}} \quad (18)$$

The corresponding deformation in z-direction is:

$$\Delta z_{ped,t}(x) = \Delta elev.x \quad (19)$$

The bending of the torque tube due to the temperature gradient contributes towards the same direction as the bending due to gravity. Equation (20) shows the displacement of the facets in z-direction:

$$\Delta z_{tube,t}(x, \Delta t) = \frac{x.(1 - \Delta t.\alpha)}{D_{torquetube}} \quad (20)$$

4.3. Superimposed deformations of reflective surface of the heliostat:

The deformation of the heliostat as a whole is the sum of all the before derived deformations. As the deformations do not influence each other, the equations can be linearly superimposed as follows:

$$z(x, y, elev, \Delta t_{ped}, \Delta t_{tube}) = \underbrace{\Delta z_{ped,g} + \Delta z_{tube,bending,g} + \Delta z_{tube,torque,g} + \Delta z_{truss,g}}_{gravitation} + \underbrace{\Delta z_{ped,t} + \Delta z_{tube,t}}_{\text{¨}temperature}$$

……. (21)

Finally, with all the values put in, the deformation of the concentrator plane from the original shape (z=0) is obtained (equation 22). In order to simplify the equation, polynoms of up to third order were used as approximations for all the equations except for the analytical solutions for the pedestal. The units of the x- and y-values are meters, the

elevation is in radians, the temperature difference in Kelvin and the unit of the z-direction is millimeters.

$$z(x, y, elev, \Delta t_{ped}, \Delta t_{tube}) = -0.459.\cos(elev + 60°).x$$
$$+(0.028.|y|^3 - 0.4178.y^2 - 0.0572.|y|).\sin(elev)$$
$$-0.0309.|y|.\cos(elev).x$$
$$+(0.0095.|x|^3 - 0.1288.x^2 - 0.0404.|x|).\sin(elev)$$
$$+0.08.\Delta t_{ped}.x$$
$$-0.0148.\Delta t_{tube}.y^2$$

…… (22)

A Matlab program was done to calculate the deformation of reflective surface of the heliostat with a fixed elevation angle and temperature difference.

5. Results and discussion:

In (Fig.9), the heliostat takes vertical position with *elev.* = 0. In comparing the deformation of the heliostat when *elev.* = 90 ° (Fig.10), we note that the deformations are more important in this case since gravitational loads increase with increasing the elevation angle and deformation take a symmetrical shape . The deformation of the reflective surface of the heliostat due to temperature is of the order of a few millimeters which do not considerably affect the performance of the heliostat

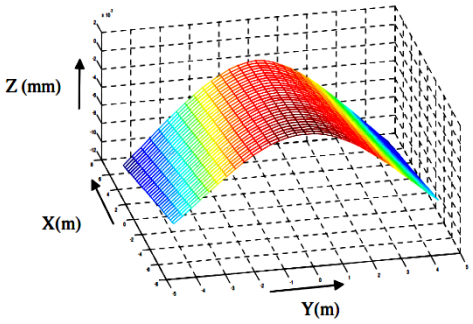

Fig.9: Heliostat deformation (*elev.=0°)*

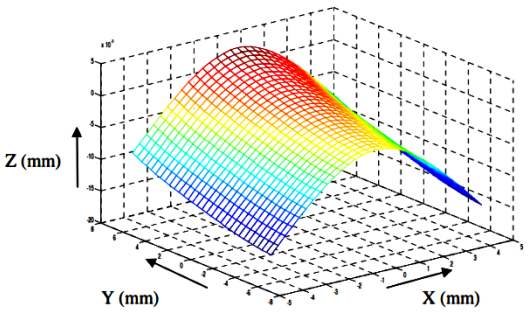

Fig.10: Heliostat deformation (*elev.*=90°)

6. Conclusion:

From the results obtained, it is clear that several parameters influence the heliostat deformation due to gravitational loads. It remains to introduce for future work dynamic wind loads that are predominant in the design of heliostats. The components of the heliostat which accentuate the change in shape of the reflecting surface of the heliostat are the support tube and trusses. It is therefore necessary to change the shapes of these two components without increasing weight or reduce their weight using composite materials.

References:

[1] Stefen Ulmer, Influence of cost reduction measures on beam quality of a large-area heliostat, platforma solar de Almeria-spain, 1998.

[2] Gregory J. Kolb, Scott A. Jones, Matthew W. Donnelly, David Gorman, Robert Thomas, Roger Davenport, and Ron Lumia, Heliostat cost reduction study, Sandia Laboratory, USA, 2007.

[3] Edgar Teufel, Reiner Buck, Andreas Pfahl, Georg Böing, and Jens Kunert, Dimensioning of Heliostat Components under Wind and Gravity Load: the Map Approach, German Aerospace Center (DLR),

[4] James E. Pacheco, Final Test and Evaluation Results from the Solar Two Project, Sandia National Laboratories, USA. 2002

[5] Francisco J. Collado, One-point fitting of the flux density produced by a heliostat, Solar energy , 2010.
[6] Viorel Badescu , Theoretical derivation of heliostat tracking errors distribution, science-direct- Solar energy, 2008
[7] Beitz W., Küttner K.-H.: "Dubbel - Taschenbuch für den Maschinenbau", 15. Auflage, Springer Verlag, Berlin, Heidelberg, 1986